CHEMICAL ENGINEERING TRANSACTIONS Volume 17, 2009
Editor Sauro Pierucci
 ISBN 978-88-95608-01-3 ISSN 1974-9791
DOI: 10.3303/CET0917092

Diffuse-Interface Modeling of Liquid-Vapor Phase Separation in a van der Waals Fluid

A.G. Lamorgese† & R. Mauri‡
†CTR, Stanford University, Stanford, CA 94305, USA
‡DICCISM, Università di Pisa, Via Diotisalvi 2, 56126 Pisa, Italy

We simulate liquid-vapor phase separation in a van der Waals fluid that is deeply quenched into the unstable range of its phase diagram. Our theoretical approach follows the diffuse-interface model, where convection induced by phase change is accounted for via a non-equilibrium (Korteweg) force expressing the tendency of the liquid-vapor system to minimize its free energy. Spinodal decomposition patterns for critical and off-critical van der Waals fluids are studied numerically, revealing the scaling laws of the characteristic lengthscale and composition of single-phase microdomains, together with their dependence on the Reynolds number. Unlike phase separation of viscous binary mixtures, here local equilibrium is reached almost immediately after single-phase domains start to form. In addition, as predicted by scaling laws, such domains grow in time like $t^{2/3}$. Comparison between 2D and 3D results reveals that 2D simulations capture, even quantitatively, the main features of the phenomenon.

1. Introduction

We present simulations of isothermal liquid-vapor spinodal decomposition of a van der Waals fluid, occurring after quenching it from a single-phase equilibrium state to the unsteady two-phase region of its phase diagram, showing that the process is governed by the density gradient-driven non-equilibrium Korteweg body force.

Although experiments and simulations on liquid-vapor phase separation have been carried out in the past (Yamamoto and Nakanishi, 1996; Beysens et al., 2002; Borcia and Bestehorn, 2007; Oprisan et al., 2008), none of these previous works has focused on spinodal decomposition systematically. In this work, applying the diffuse-interface model (Felderhof, 1970; Antanovskii, 1996; Anderson et al., 1998), we report on liquid-vapor spinodal decomposition in 2D and 3D for an off-critical van der Waals fluid as a function of a convection parameter expressing the relative magnitude of capillary to viscous forces. We show that, at the late stages of the process, the mechanism of growth is convection-driven coalescence with a $\frac{2}{3}$ power-law scaling for the characteristic size of single-phase microdomains, in agreement with dimensional analysis (Siggia, 1979; Furukawa, 1994) and experimental measurements (Beysens et al., 2002).

In this article, we recall in Section 2 definitions of quantities and non-dimensional parameters of the diffuse-interface model. Then, in Section 3, after a brief description of our numerical method, spinodal decomposition patterns and the scaling law for the typical domain size and composition of single-phase microdomains are discussed. At the end, a

Please cite this article as: Lamorgese A. and Mauri R., (2009), Diffuse-interface modeling of liquid-vapor phase separation in a van der waals fluid, Chemical Engineering Transactions, 17, 549-554 DOI: 10.3303/CET0917092

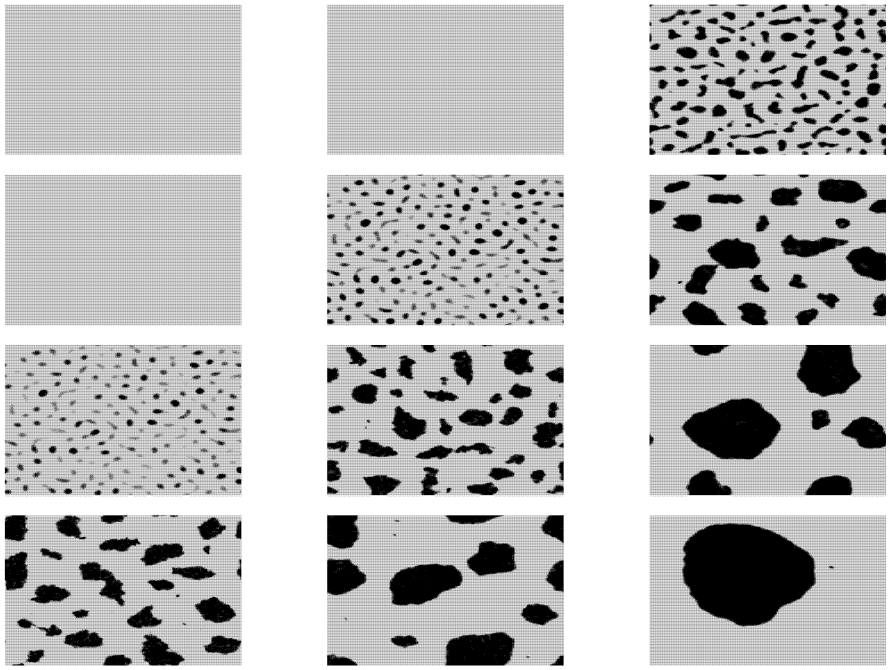

Figure 1: Liquid-vapor spinodal decomposition of an off-critical van der Waals fluid (with $\tilde{\rho}_0 = 1.3$) at different non-dimensional times (diffusive scaling) $\tilde{t} = 3\,10^{-3}$, 10^{-2} and $5\,10^{-2}$, with $\mathscr{R} = 1$, 10, 10^2 and 10^3 from top to bottom.

few conclusions are drawn.

2. The Governing Equations

The derivation of the governing equations has been presented elsewhere (Lamorgese and Mauri, 2008). There, the equations of motion were obtained rigorously, coupling the van der Waals equation of state with the fundamental conservation principles and invoking irreversible thermodynamics. Also, the governing equations were made dimensionless based on both a diffusive scaling (which is relevant at the beginning of phase separation) and an acoustic, or convective, scaling (which is relevant at the late stage of phase separation). We remind below basic definitions of non-dimensional groups that emerge under the acoustic scaling. Accordingly, defining a reference speed of sound, $u_s = (RT_c/M_W)^{1/2}$, we set:

$$\tilde{\mathbf{x}} = \frac{\mathbf{x}}{L}, \quad \tilde{t} = \frac{u_s t}{L}, \quad \tilde{\mathbf{u}} = \frac{\mathbf{u}}{u_s}, \quad Re = \frac{\rho_c u_s L}{\eta_I}, \quad \beta = \frac{N_A d^3}{M_W}\rho_c, \tag{1}$$

$$\tilde{\rho} = \frac{\rho}{\rho_c}, \quad \tilde{p} = \frac{p}{\rho_c R T_c/M_W}, \quad \tilde{T} = \frac{T}{T_c}. \tag{2}$$

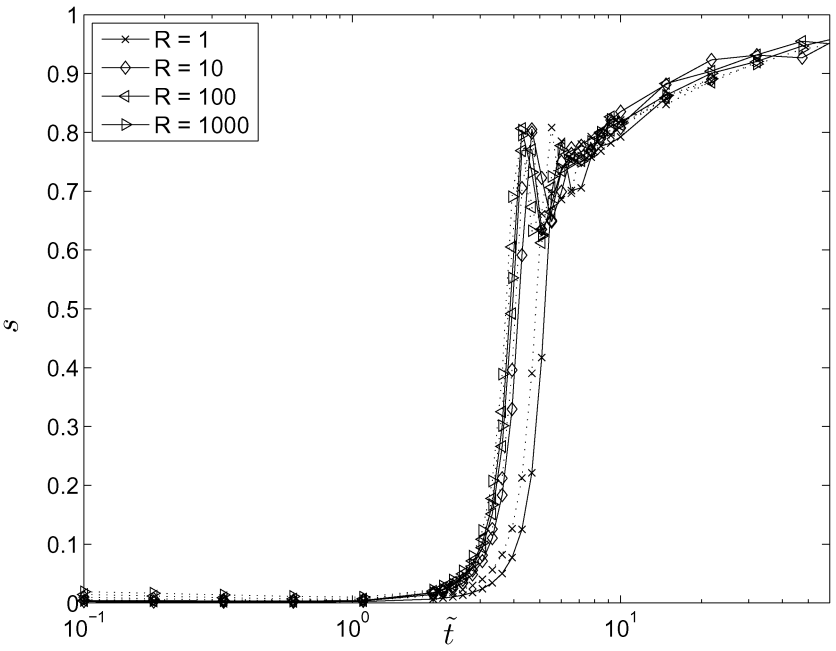

Figure 2: Separation depth vs. time (acoustic scaling) for different values of $\mathscr{R} = 1$, 10, 100, 1000 from 2D simulations with $\tilde{\rho}_0 = 1.3$ (solid) vs. 3D simulation results (dotted).

Here, d, N_A and M_W denote a molecular diameter, the Avogadro number and the molecular weight, respectively, whereas ρ_c and T_c are the critical density and temperature, and $p_c = \rho_c R T_c / M_W$ is the pressure at critical conditions if the fluid were a perfect gas (R being the gas constant), and β is an $O(1)$ density ratio. Re is an acoustic Reynolds number which can be used to define an interfacial Reynolds number as

$$\mathscr{R} = (ReCn)^2 = \left(\frac{\rho_c u_s a}{\eta_I} \right)^2 , \tag{3}$$

where η_I is the viscosity of the liquid phase and where the Cahn number, $Cn = a/L$, is the ratio of the interface thickness a to the macro length scale L. In fact, it can be shown that the non-dimensional parameter $\mathscr{R}$ can be defined independently as the ratio of capillary-to-viscous forces (i.e. as an inverse capillary number). In the governing equations, all external forces, and buoyancy in particular, were assumed to be negligible. In other words, drop and bubble sizes ℓ are small compared to the capillary length, i.e., $\ell \ll \sqrt{\sigma / g\,(\rho_I - \rho_{II})}$ (with σ the surface tension, g the gravity field and with I and II denoting the liquid and vapor phases at equilibrium), which amounts to assuming that the Bond number is very small. Also, for the sake of simplicity, we assumed $\beta = 1$.

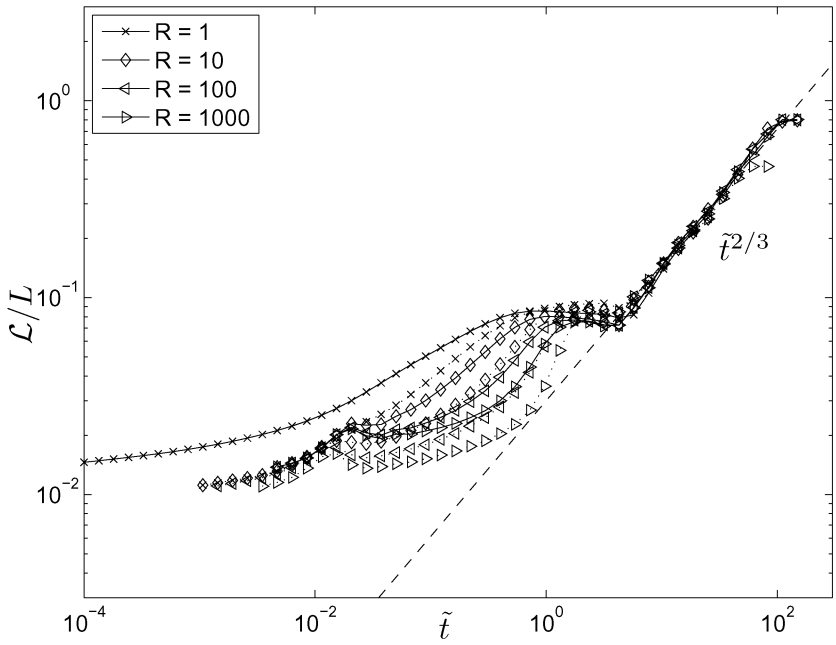

Figure 3: Integral scale vs. time (acoustic scaling) for different values of $\mathscr{R} = 1, 10, 100, 1000$ from 2D simulations with $\tilde{\rho}_0 = 1.3$ (solid) vs. 3D simulation results (dotted).

3. Numerical Results

Our numerical methods are based on previous works by Nagarajan et al. (2003, 2007). Accordingly, the governing equations were discretized using a structured, staggered arrangement of the conserved variables, with spatial derivatives computed via sixth-order compact finite differences (Lele, 1992). Temporal advancement was effected via a third-order Runge-Kutta scheme.

3.1 Liquid-vapor spinodal decomposition

We investigated liquid-vapor spinodal decomposition of a van der Waals fluid which is instantaneously quenched into the unstable region of its phase diagram. The simulations were conducted at $\tilde{T} = 0.9$, for negligible Bond number and for different values of $\mathscr{R}$, assuming an infinite expanse of fluid (modeled via periodic boundary conditions). At this temperature, a representative vapor-liquid viscosity ratio was chosen to be $r = 10^{-3}$. Initially, we assumed quiescent conditions with a density field being the sum of a Gaussian white noise superposed on a uniform constant density $\rho = \rho_0$. We chose values of $\tilde{\rho}_0 = 0.7, 1.042, 1.3$ in the spinodal range, i.e., $\tilde{\rho}_0 \in [\tilde{\rho}_s^{II}, \tilde{\rho}_s^{I}]$, where $\tilde{\rho}_s^{I} = 1.39$ and $\tilde{\rho}_s^{II} = 0.654$ denote the liquid and vapor spinodal densities at the given temperature. (For a van der Waals fluid these values are easily found by solving the algebraic relation $\tilde{\rho}(3-\tilde{\rho})^2 = 4\tilde{T}$.) Specifically, $\tilde{\rho}_0 = 1.042$ is the critical density, while $\tilde{\rho}_0 = 0.7$ and $\tilde{\rho}_0 = 1.3$

correspond to vapor-rich and liquid-rich mixtures, respectively. As expected, we observed that the phase-ordering process after the critical quench $\tilde{\rho}_0 = 1.042$ is characterized by the formation of bicontinuous structures, which subsequently grow and coalesce. For the off-critical quench, $\tilde{\rho}_0 = 1.3$ (Fig. 1), the phase separation pattern consists of a random collection of rapidly coalescing pseudo-spherical nuclei of the minority phase, surrounded by the majority phase. Only after the first spinodal pattern is formed (i.e., a bicontinuous pattern for the critical quench, or a random collection of nuclei for the off-critical quench), do the single-phase domains start to grow and coalesce, at an increasing rate for larger $\mathscr{R}$. As a quantitative characterization of the influence of the convection parameter $\mathscr{R}$ on the average phase composition of the two-phase fluid, we defined the separation depth, s, measuring the "distance" of the single-phase domains from their equilibrium state (Vladimirova et al., 1998) as

$$s = \left\langle \frac{\rho(\boldsymbol{x}) - \rho_0}{\rho_{eq}(\boldsymbol{x}) - \rho_0} \right\rangle, \tag{4}$$

where ρ_0 is the initial mean density, and the brackets indicate volume and ensemble averaging. Here, ρ_{eq} denotes the steady-state density of the liquid phase, ρ_I, or of the vapor phase, ρ_{II}, depending on the local density $\rho(\boldsymbol{x})$, i.e.,

$$\rho_{eq}(\boldsymbol{x}) = \begin{cases} \rho_I, & \text{if } \rho(\boldsymbol{x}) > \rho_0, \\ \rho_{II}, & \text{if } \rho(\boldsymbol{x}) < \rho_0. \end{cases} \tag{5}$$

Figure 2 shows the temporal evolution (in acoustic time units) of the separation depth for the off-critical quench $\tilde{\rho}_0 = 1.3$ for $\mathscr{R} = 1,\ 10,\ 100,\ 1000$. The solid curves in this figure were obtained from 2D simulations on a 256^2 grid, whereas the dotted lines are from 3D simulations on a 128^3 grid. This figure shows remarkable quantitative agreement between the two sets of curves.

Next, we studied the rate of coarsening as reflected in the growth law for the integral scale

$$\mathcal{L}(t) = \frac{1}{\rho_{rms}^2} \sum_{\mathbf{k}} \frac{\langle |\hat{\tilde{\rho}}_{\mathbf{k}}|^2 \rangle}{|\mathbf{k}|}, \tag{6}$$

where $\tilde{\rho} = \rho - \langle \rho \rangle$, ρ_{rms} is the root-mean-squared value of ρ, hats denote Fourier transforms, while the brackets denote averaging over a shell in Fourier space at fixed $k = |\mathbf{k}|$. As can be seen in Fig. 3, during the first stage of the process the rate of coarsening is strongly influenced by the chosen value for the convection parameter, until sharp interfaces are formed. Then, domains stop growing, concomitant to their composition rapidly reaching local equilibrium. Finally, during the latest stage, growth is driven by inertial forces and is characterized by a $\frac{2}{3}$ power-law behavior, in agreement with predictions based on simple dimensional analysis (Siggia, 1979; Furukawa, 1994). So, first there is a time delay, with no detectable liquid-vapor phase separation. Then, during the second and third stages, first the system reaches local equilibrium (with the formation of nuclei having sharp interfaces), and then these nuclei start to grow. This is in contrast with phase separation in viscous liquid binary mixtures, where the two events occur simultaneously. There, after the (delayed) onset of phase separation, local equilibrium is reached

well after the appearance of nuclei with sharp interfaces, through a process of composition relaxation of the nuclei that is concomitant to their temporal growth. In addition, in liquid-liquid phase separation, capillary forces are balanced by viscous forces, leading to a linear growth law of the nuclei sizes, while for liquid-vapor phase transition, capillary forces are balanced by inertial forces, leading to a $\frac{2}{3}$ power-law behavior.

References

Anderson D. M., McFadden G. B. and Wheeler A. A., 1998, Diffuse-interface methods in fluid mechanics, Annu. Rev. Fluid Mech. 30, 139–165.

Antanovskii L. K., 1996, Microscale theory of surface tension, Phys. Rev. E 54, 6285–6290.

Beysens D., Garrabos Y., Nikolayev V. S., Lecoutre-Chabot C., Delville J.-P. and Hegseth J., 2002, Liquid-vapor phase separation in a thermocapillary force field, Europhys. Lett. 59 (2), 245–251.

Borcia R. and Bestehorn M., 2007, Phase-field simulations for drops and bubbles, Phys. Rev. E 75, 056309.

Felderhof B. U., 1970, Dynamics of the diffuse gas-liquid interface near the critical point, Physica 48, 541–560.

Furukawa H., 1994, Role of inertia in the late stage of the phase separation of a fluid, Phys. A 204, 237–245.

Lamorgese A. G. and Mauri R., 2008, Diffuse-interface modeling of liquid-vapor phase separation in a van der Waals fluid, submitted.

Lele S. K., 1992, Compact finite-difference schemes with spectral-like resolution, J. Comput. Phys. 103, 16–42.

Nagarajan S., Lele S. K. and Ferziger J. H., 2003, A robust high-order compact method for large-eddy simulation, J. Comput. Phys. 191, 392–419.

Nagarajan S., Lele S. K. and Ferziger J. H., 2007, Leading-edge effects in bypass transition, J. Fluid Mech. 572, 471–504.

Oprisan A., Oprisan S. A., Hegseth J., Garrabos Y., Lecoutre-Chabot C. and Beysens D., 2008, Universality in early-stage growth of phase-separating domains near the critical point, Phys. Rev. E 77 (5), 051118.

Siggia E., 1979, Late stages of spinodal decomposition in binary mixtures, Phys. Rev. A 20, 595–605.

Vladimirova N., Malagoli A. and Mauri R., 1998, Diffusion-driven phase separation of deeply quenched mixtures, Phys. Rev. E 58, 7691–7699.

Yamamoto R. and Nakanishi K., 1996, Computer simulation of vapor-liquid phase separation, Mol. Sim. 16, 119–126.